A New Constructed Geometry of A Switched Reluctance Motor for Reduced Torque Ripple

تشكيل هندسى جديد لمحرك المعاوقه الانتقاليه للتقليل من تذبذب العزم

M. Hamouda, A. R. A. Amin and E. Gouda
Electrical Engineering Department, Mansoura University, Mansoura 35516, Egypt.
e-mail: m_hamouda26@mans.edu.eg

الخلاصة

يقدم هذا البحث مقترح جديد لاعادة تشكيل محرك المعاوقه الانتقاليه وذلك لتحسين موجة العزم الكلى للمحرك وتقليل التذبذب المُنتج على موجة العزم، ولهذا الغرض يوضح البحث الفرق بين المحرك التقليدى والنموذج المقترح الجديد من خلال دراسة الاداء لكل منهما فى حالة السكون والديناميكية باستخدام برنامج **MATLAB** وبرنامج **Finite Element Analysis (FEA)**. برنامج **FEA** تم استخدامه للحصول على المنحنيات المغناطيسية للمحرك عند قيم تيارات مختلفة مع تغير وضع العضو الدوار. ومن خلال المنحنيات المغناطيسيه تم عمل برنامج محاكاه للمحرك باستخدام **MATLAB/Simulink Package**. تم دراسة تغير شكل الاقطاب على اداء المحرك، ومقارنة النتائج النظرية بالمعملية.

Abstract

This paper presents a proposed structure model for a 6/4 switched reluctance motor (SRM) in order to improve the average torque production with ripple minimization. Therefore, it describes the differences between the standard 6/4 pole SRM and the proposed one in static and dynamic characteristics using Finite Element Analysis (FEA) and Matlab/Simulink package. FEA is used to obtain the nonlinear magnetization characteristics of the SRM to be used in Matlab Simulation model. The effects of different poles construction on the SRM performance are investigated. Validation of the computational methods is carried out by comparing the calculated static characteristics with the ones measured experimentally on 6/4 SRM prototype. The obtained results illustrate minimized torque ripples and better performance for the proposed SRM. A drive system for the SRM is implemented and a series of results are illustrated and discussed.

Index Terms

Pole shape, SRM, Torque Ripple, FEM, ANN, Matlab.

I. Introduction

The SRM has a prime feature of simple construction. It does not have permanent magnets (PMs), brushes and commutators. The stator consists of salient poles of steel laminations. With no rotor windings, the rotor is a piece of steel (laminations) that is shaped to form salient poles making it well-suited for high speed operation [1]-[3]. The SRM promises a reliable and low-cost variable-speed drive. It will certainly take place of many drives in the short future [4].

One of the SRM's major problems is the torque ripple which causes increased undesirable acoustic noise and possibly speed oscillations. It is not necessary to determine the torque ripple and acoustic noise for the system in all cases, but it depends on the application [5]. There are mainly two methods for reducing the torque ripple. One method is improving the magnetic design of the SRM, while the other method is to use complicated electronic control techniques [6].

The electronic approach is based on optimizing the control parameters, which include the supply voltage, turn-on and turn-off angles, and current level. Torque ripple reduction through electronic control may lead to a reduced average torque, since the motor capabilities are not being fully utilized at all power levels [5].

For decades, there has been much research directed toward the reduction of this

Received: 31 March, 2015 – Accepted: 3 August, 2015

undesirable torque ripple. For instance frequently, the stator and rotor pole arcs have been optimized as design parameters [1], [7], [8]. Another research group has tried to control both the switching on and off angles and the driving currents by using dynamic finite element analysis [9]. Several attempts have been made to optimize the geometric shapes of the stator and rotor pole by slanting the stator pole face [10], by using the relative eccentricity of the stator and rotor poles with a non-uniform air-gap [11], and by using rotor poles having notches [12].

The optimization of control method and design of motor geometry must be performed simultaneously [11], bearing in mind that actions leading to reduction of torque ripple can be at the expense of some output characteristics of the SRM, e.g. efficiency.

The main idea for the reduction of the torque ripple comes from the fact that the torque and current profiles are only a function of the inductance pattern if the exciting voltage and the switching on and off times for each phase are fixed [11]. changing the air-gap profile between the stator and rotor poles controls inductance pattern. Or changing the rotor and stator pole shapes to control the linkage flux and hence the inductance pattern. Having observed this possibility of control, this paper optimizes the stator pole face and the pole shoe attached to the lateral face of rotor pole. This optimization increases the average torque with significant reduction of ripples without changing the pole arcs and switching on and off times. The two dimensional 2D-FEM is used to obtain the optimal shape of the proposed model.

This paper is organized as follows: Section II presents the SRM nonlinear mathematical model; Section III describes the SRM configurations and magnetic circuit geometry; However the optimum dimensions are calculated in Section IV; Section V shows the static characteristics obtained from FEA; Section VI describes the simulated dynamic characteristics using matlab/Simulink; Section VII presents an estimation of core losses; Section VIII describes the experimental validation; and Section IX gives the conclusions drawn from this research.

II. Mathematical Model

The mathematical model that predicts the dynamic and steady state characteristics of the SRMs is described by the following set of equations. The symbols V_k , ψ_k , R_k , I_k, , T_k , T_e , θ, ω, J, B, T_L , W'_m and m are the voltage, flux linkage, resistance, current, phase torque, electromagnetic torque, rotor position angle, speed, moment of inertia, friction coefficient load torque, magnetic field co-energy and number of motor phases respectively [2], [5].

$$V_k = R_k I_k + \frac{d\psi_k}{dt} \quad \textbf{(1)}$$

$$\psi_k = \psi(I_1, \dots\dots) = \psi(I_k, \theta) \quad \textbf{(2)}$$

$$\psi_k = \psi(I_k, \theta) = L(I_k, \theta)\, I_k \quad \textbf{(3)}$$

$$T_k = \frac{dW'_m(I_k,\theta)}{d\theta} = T(I_k, \theta) = \frac{1}{2} i^2 \frac{dL}{d\theta} \quad \textbf{(4)}$$

$$T_e = \sum_{k=1}^{m} T(I_k, \theta) = T_L + B\omega + J\frac{d\omega}{dt} \quad \textbf{(5)}$$

$$\omega = \frac{d\theta}{dt} \quad \textbf{(6)}$$

The mutual inductance among phase windings can be neglected to simplify (2) to (3) [13]. The torque ripple, average torque and efficiency values are calculated as:

$$T_r\% = \frac{max(T_i) - min(T_i)}{T_{avg}} .100 \quad \textbf{(7)}$$

$$T_{avg} = \frac{1}{T}\int_0^T T_{inst.}\, dt \quad \textbf{(8)}$$

$$\eta\% = \frac{T_{avg} \cdot \omega_{avg}}{V_{avg} \cdot I_{avg}} .100 \quad \textbf{(9)}$$

Where, $max(T_i)$, $min(T_i)$, T_{avg} , ω_{avg} , I_{avg} and V_{avg} are the maximum and minimum values of instantaneous torque, average electromagnetic torque, average speed, average supply current and average voltage respectively.

Torque dip is a measure of the torque ripple. It is the difference between the peak torque of a phase and the torque at an angle where two overlapping phases produce equal

torque at equal current levels. This is due to the deficiency of the incoming phase in supplying the necessary torque in those rotor positions [5].

III. SRM Configurations

The basic dimensions of the Standard 6/4 SRM is given in Table I. The standard SRM magnetic circuit structure and main geometry configurations are shown in Fig. 1(a), while the proposed one is illustrated in Fig. 1(b). The proposed SRM has two foots one is attached to the stator pole and the other to the rotor pole. The stator foot has two different dimensional parameters which are the stator foot angle (β_{fs}) and the stator foot height (h_{fs}). On the other hand, the rotor foot has another two different dimensional parameters which are the rotor foot angle (β_{fr}) and the rotor foot height (h_{fr}) as shown in Fig.1 (b). These dimensional parameters are needed to be optimized seeking for optimal operation of the proposed SRM. The optimization that includes improving the average torque with reducing torque ripple is presented in the following section.

IV. Optimum Dimensions Calculation

The optimum dimensions of the proposed model are calculated using 2D-FEM throughout an optimization technique which is illustrated as a flowchart in Fig. 2. The technique depends on changing the dimensions which under optimization in steps and choosing the optimum value associated with higher torque production and minimum ripples.

With an initial value for ($h_{fs} = 3$ mm), the change of β_{fs} affects the average torque and ripples. It can be noted that the minimum torque dip and the minimum static torque ripples has been observed with $\beta_{fs} = 43°$ as illustrated in Fig. 3.

According to the optimum value of $\beta_{fs} = 43°$, and with changing h_{fs}, the minimum torque dip is achieved at $h_{fs} = 4.5$ mm as observed from Fig.4.

Adding a pole shoe to the rotor in addition to the stator foot reduces the minimum inductance region and increases the flat torque region as discussed in section V.

The best choice taking into consideration the actual shape of the current waveform and the switch on and off times will be $\beta_{fr} = 38°$ over the rotor pole pitch of 45° as shown in Fig. 5. This choice is the optimum value of β_{fr} with $\beta_r = 30°$ instead of $\beta_r = 33°$ to save the material volume and cost.

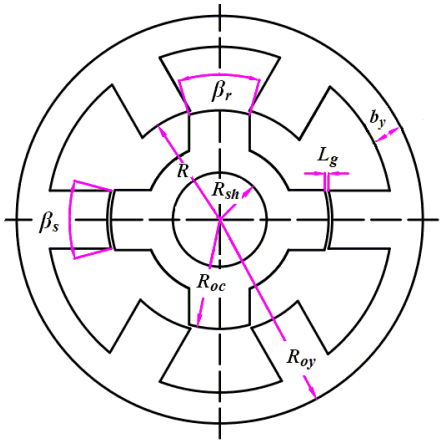

(a) Standard 6/4-pole SRM

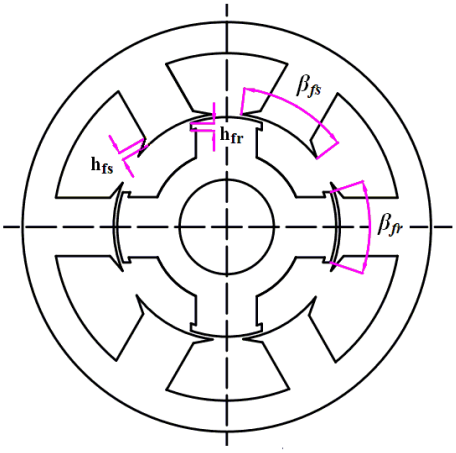

(b) Proposed SRM

Fig. 1 SRM configurations

V. Static Characteristics Calculation

The flux linkage calculation of one phase and static torque characteristics as a function of rotor position (θ) and current (i) is mainly the first step to predict SRM performance. These characteristics are obtained using 2D-FEM for magneto-static field analysis and stored in lookup tables $\psi(\theta, i)$ and $T(\theta, i)$.

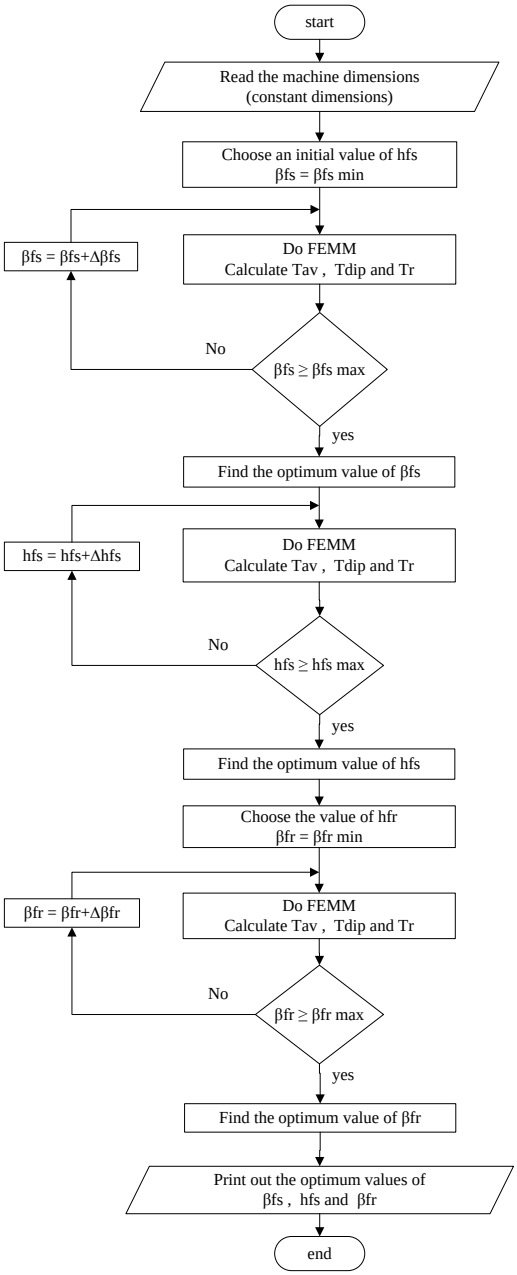

Fig. 2 Flowchart of the optimization technique

Angle $\theta = 0°$ represents unaligned position and angle $\theta = 45°$ describes aligned position, the rotor positions (θ) are defined by mechanical degrees. At unaligned position, the phase inductance has minimum value because of the large air-gap as shown in Fig. 6. The flux linkage is linear behavior, and magnetic saturation is unlikely to occur at this position until a pair of stator and rotor poles exhibits overlap. In the partial and fully overlap regions, magnetic field density tends to saturate tip and body of the poles at high current levels making flux linkage a nonlinear function of position and current.

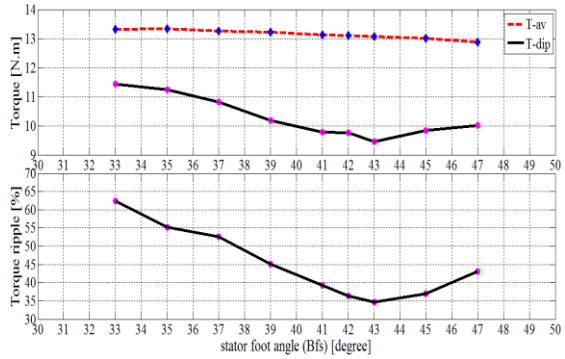

Fig. 3 The effect of changing the stator foot angle.

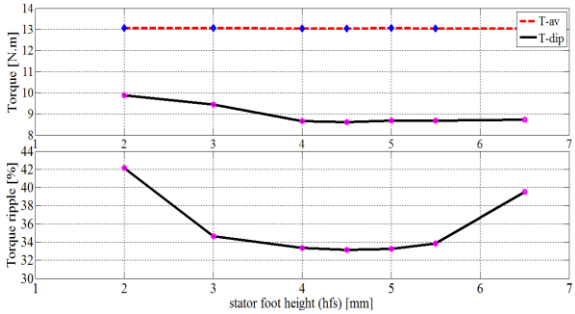

Fig. 4 The effect of changing the stator foot height.

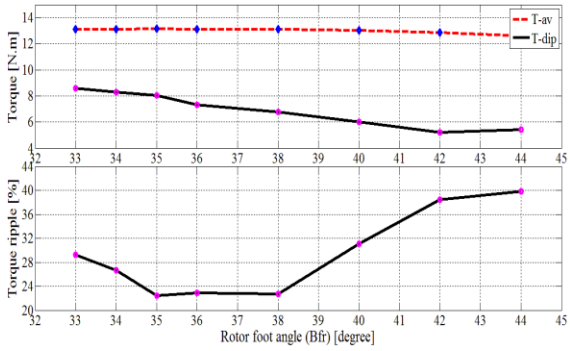

Fig. 5 The effect of changing the rotor foot angle.

The proposed SRM has greater magnetic field co-energy as shown in Fig. 7 which demonstrates more torque production [14].

Figures 8 and 9 show the flux linkage and static torque characteristics for the standard and proposed SRMs respectively.

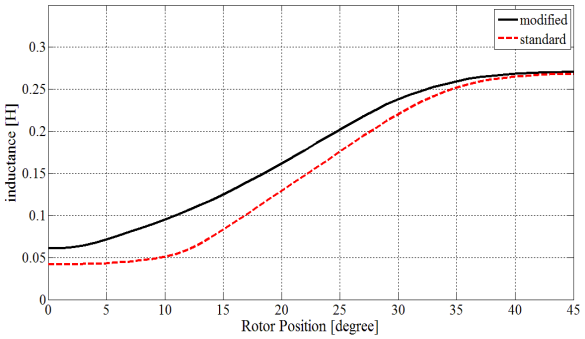

Fig. 6 The calculated inductance pattern using FEM.

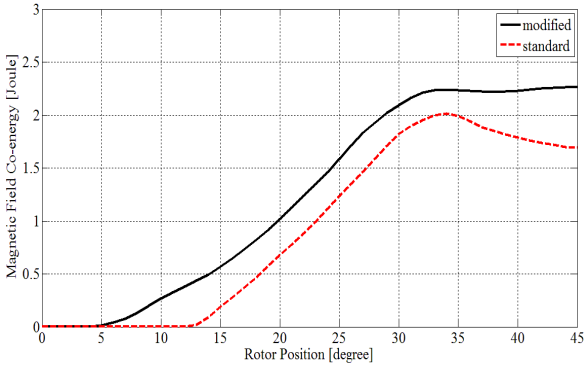

Fig. 7 The calculated magnetic field Co-energy using FEM.

The flux lines and the flux density distribution at $\theta = 20°$ with an exciting current of $6(A)$ are shown in Fig. 8(a) and Fig.9(a). The pole shoe on rotor and that one on stator have been saturated due to their small cross section area offered against the rated ampere turns.

VI. Dynamic Characteristics Calculation

Dynamic simulation is carried out based on the mathematical model mentioned above from (1) to (6). These equations are solved simultaneously using software Matlab/Simulink. Rotor position sensing unit gives information about rotor position. The electronic control block defines the switching state for each phase which are the switch on (θ_{on}) and switch off (θ_{off}) angles. The voltage $+V$ is applied when $\theta_{on} \leq \theta \leq \theta_{off}$ and the voltage is $-V$ when $\theta \geq \theta_{off}$. The phase currents of the motor were limited by chopping process [15].

The simulation is carried out to discuss the performance of the standard and proposed SRM with a current limiter, a conventional PI speed controller and using ANN.

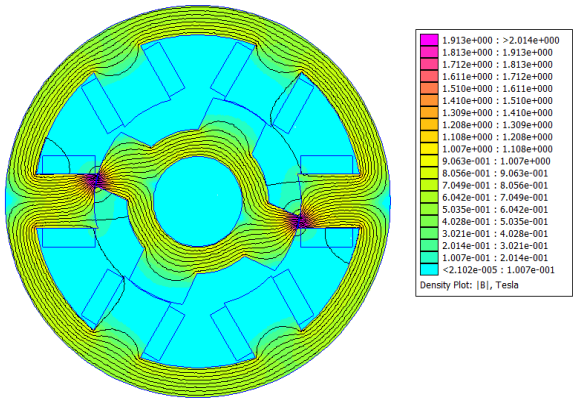

The flux density distribution at 20^o with 6 (A) for standard SRM.

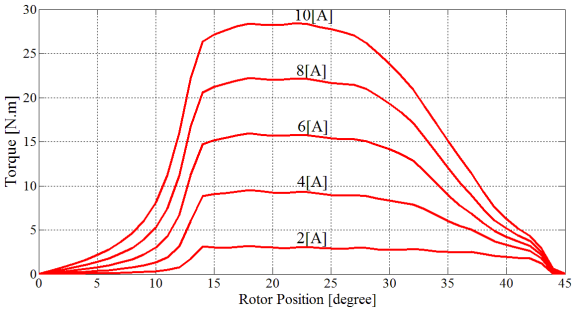

a. Static torque characteristics for standard SRM.

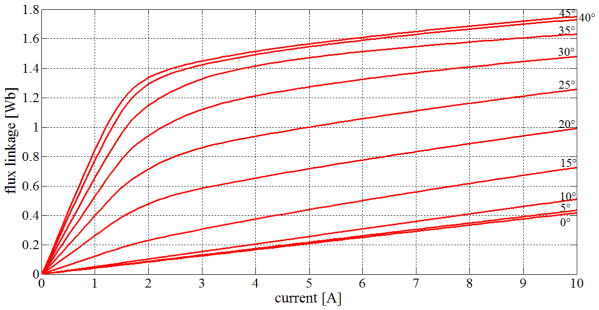

b. Flux linkage characteristics for standard SRM.

Fig. 8 the calculated static characteristics using FEMM for the standard SRM.

Operating conditions for the two SRMs configurations are listed in the Table II and Table III. The supply voltage varies between positive and negative DC bus voltage (hard switching). θ_{on} is in the unaligned (minimum inductance) position and θ_{off} is determined in order to minimize torque ripple.

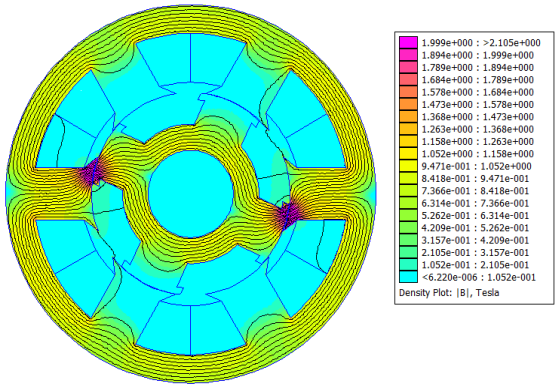

a. The flux density distribution at 20^{o} with 6 (A) for the proposed SRM.

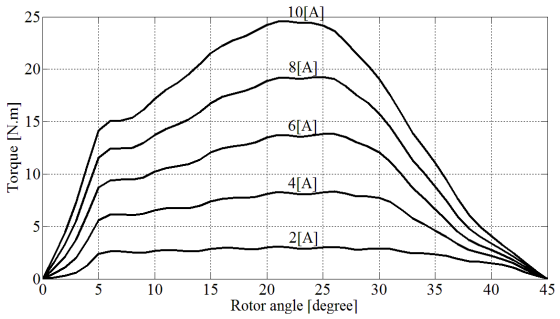

b. Static torque characteristics for the proposed SRM.

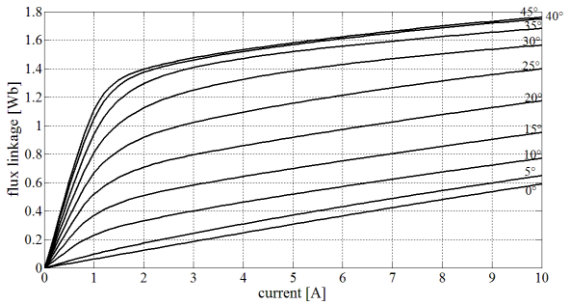

c. Flux linkage characteristics for the proposed SRM.

Fig. 9 the calculated static characteristics using FEMM for the proposed SRM model.

The matlab/Simulink model consists of three parts, the motor dynamic modeling, the controller and the position sensing unit as shown in Fig. 10. The simulation of one phase of the SRM is carried out by solving (1) to estimate the phase current. The SRMs characteristics are calculated by 2D-FEM and stored in lookup tables to be used in simulation model as shown in Fig. 11. The position sensing unit feeds the controller with the correct position for each phase. According to the phase position, the controller determines the firing angles for this phase.

A. Simulation results with current limiter only

The SRM's torque-speed characteristics are classified as series characteristics where the speed is decreased rapidly with the increased load torque as illustrated in Fig. 12. For the same switch on and switch off angles, the proposed SRM has higher speed till nearly its rated speed of about 850 (rpm). For speeds above the rated speed, the standard SRM will have the higher speeds because of the increased current at the start of the increasing inductance zone which in turn increases the produced torque. To allow the proposed SRM to operate with high speeds, it is essential to change the switch on and off angles to adapt to its new inductance pattern.

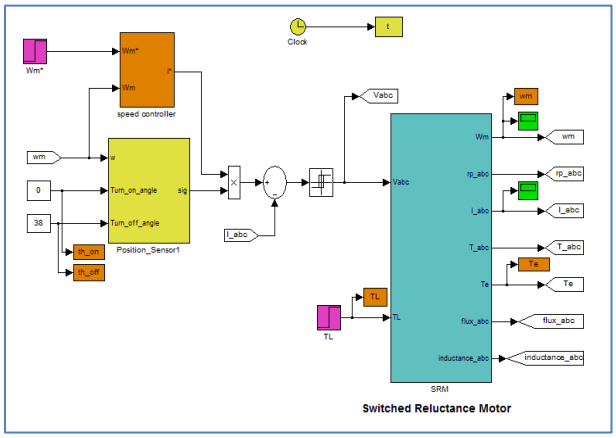

Fig. 10 Overview of the SRM model in matlab/Simulink

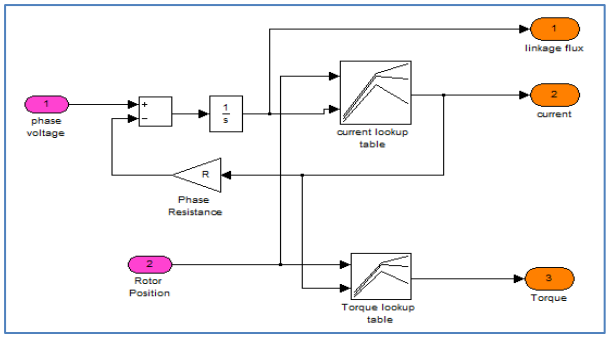

Fig. 11 Simulation of one phase of the SRM.

The SRM must be turned on early in the minimum inductance region to increase current in smaller time in order to allow the motor to produce greater torque. On the other hand, the switch off angle should be delayed as can as possible to increase the conduction period and gives more torque production. The switch off angle should be optimized to prevent the production of negative torque and also to avoid the flux commulation from two phases which may lead to more saturation and more temperature rise. The effect of changing the switch off angle on torque ripple, efficiency and output mechanical power is shown in Fig. 13. The optimum switch off angle is seen to be 38^o.

The total electromagnetic torque produced by the standard and modified SRMs is shown in Fig. 14, it is clear that the proposed SRM has reduced torque ripples and higher speed with minimum speed oscillations. The higher speed reflects the greater output mechanical power and the improved efficiency for the proposed SRM.

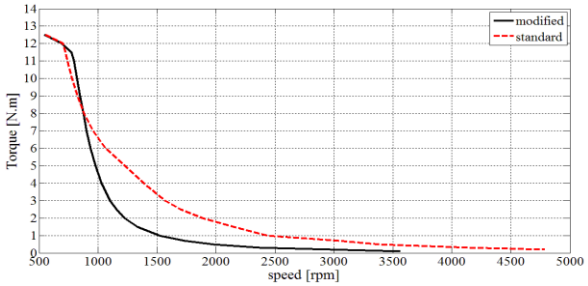

Fig. 12 Torque-speed characteristics of the SRMS.

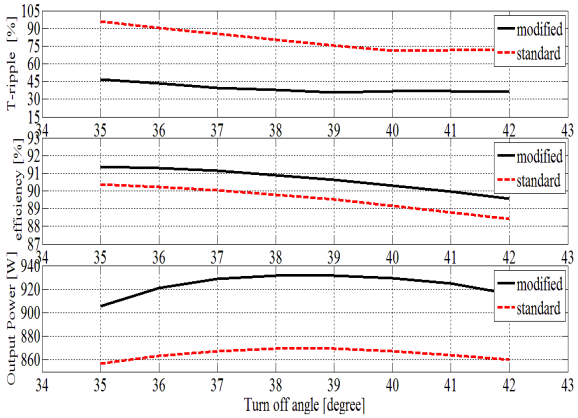

Fig. 13 The effect of changing the turn off angle with only current limiter.

B. Simulation results with PI speed controller

The performance of the SRM with a PI speed controller is different from its performance with only current limiter. The actual speed of the motor is compared with its reference value to calculate the speed difference or the error signal. This error is processed by a PI controller to determine the reference current of the motor as shown in Fig. 10. The output reference current from the PI controller has a limited value which not allowed to be exceeded.

The total electromagnetic torque produced by the standard and proposed SRM is illustrated in Fig. 15. It can be noticed that the torque ripples for the proposed SRM are significantly reduced. The speed oscillations are also decreased because it depends on the produced torque ripple and rotor inertia.

The effect of changing the switch off angle on torque ripples and efficiency is shown in Fig. 16. The minimum torque ripple is associated with θ_{off} =38^o.

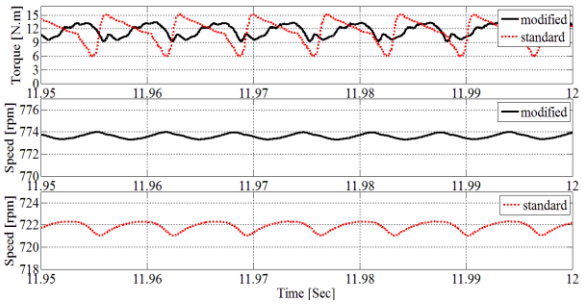

Fig. 14 Simulation results with current limiter and θ_{off} = 38°

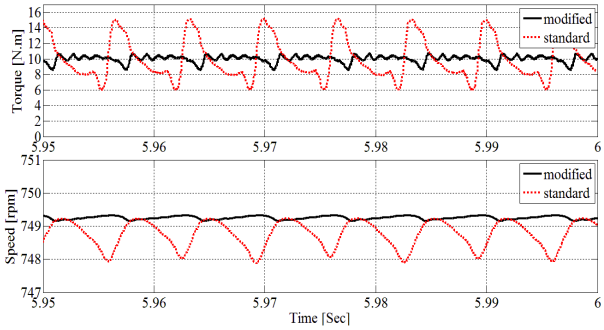

Fig.15 the electromagnetic torque and the speed ripple.

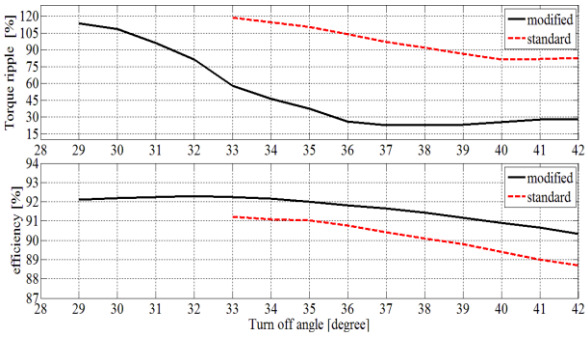

Fig.16 the effect of changing the turn off angle with speed controller.

C. Commutation angles control using ANN

Artificial neural network (ANN) is trained for online control of the switching angle [16]. The input of ANN is the torque and speed, where the switch-on and off angles are the output with constant conduction angle of 33^{o} as shown in matlab simulation block diagram in Fig.17.The network uses the Levenberg-Marquardt algorithm for training. Fig.18 shows the ANN training performance which is a plot of training error, validation error and test error. It shows that final means square error is small. The switching angles depend on both the speed and the torque (or current). Fig.19 illustrates the online control of the switch-on and off angles with the change in speed and load torque.

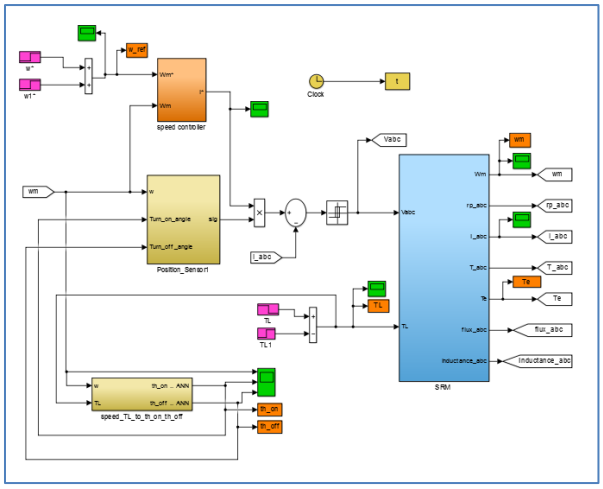

Fig.17 simulation block diagram using ANN.

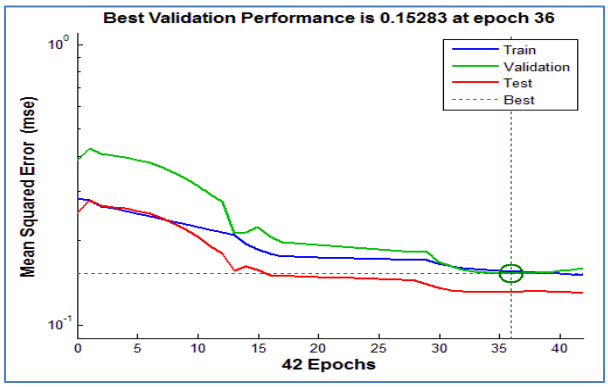

Fig.18 ANN training Performance

At low speed the current has enough time to increase after switching on so the switch on angle can be delayed. On the other hand with high speed the switch on angle must be early enough to allow the current to increase during minimum inductance region. The value of the phase current depends on the load torque. At heavy loads (greater current), the switch on angle should be earlier than its value for light loads at the same speed.

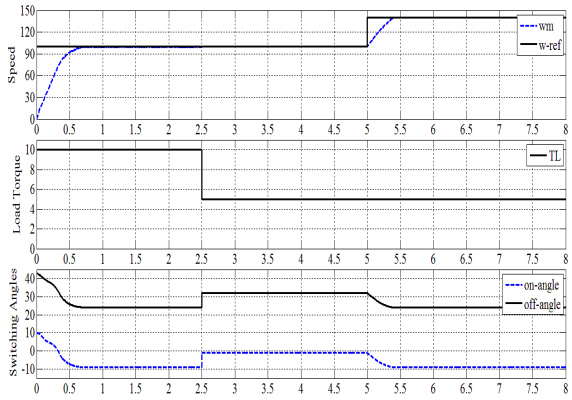

Fig.19 switching angles control with changing of load torque and speed

VII. Estimation of Core Losses

The calculation of SRM iron losses is complex because the flux waveforms are nonsinusoidal, different parts of the magnetic circuit have different waveforms and these waveforms are conditioned by the type of control used [17]. The specific core losses (W/kg) are separated into two parts (hysteresis losses and eddy current losses).

The core losses are calculated using the waveforms and time derivatives of the local flux density using (10) for each part of the machine (stator pole, stator yoke , rotor pole and rotor yoke). FEM is used to get the accurate flux density waveforms in each part in the SRMs over one cycle.

$$P_c = k_{cf} C_h f B_{max}^{a+b.B_{max}} + \frac{1}{2\pi^2} C_e \left(\frac{dB}{dt}\right)^2_{avg} \quad (10)$$

$$k_{cf} = 1 + \frac{k}{B_{max}} \sum_{i=1}^{n} \Delta B_i \quad (11)$$

Where f is the frequency. B_{max} is the maximum flux density. C_h, a, b and C_e are the Steinmetz parameters from reference [18] for M-19 steel. ΔB_i is the amplitude of the i^{th} minor loop and n is a half number of minor loops over one period of the flux density waveform.

The estimated core losses (W) for the standard and modified SRMs are 32.33/33.62 respectively with frequency equal to 50 (Hz) related to the motor speed.

VIII. Experimental Verification

The inductance of the machine winding is measured using an alternating current $i = 1$ A, while the phase resistance is premeasured by a DC supply [19]. The comparison between measured and calculated inductance pattern is shown in Fig.20.

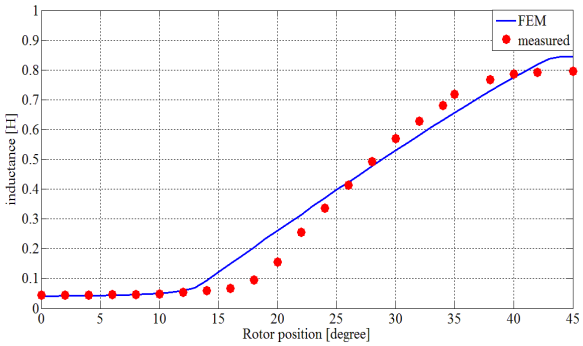

Fig. 20 Calculated and measured inductance.

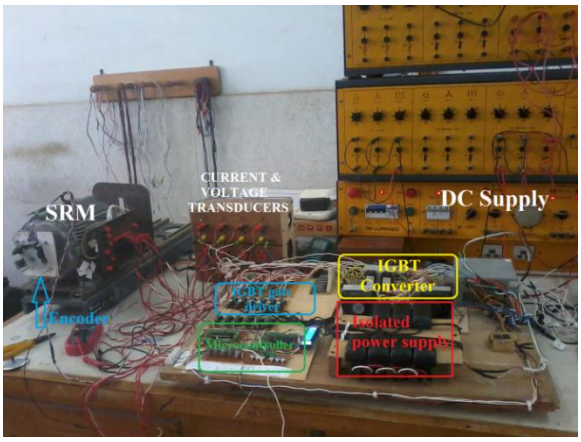

Fig. 21 The benchmark layout.

The differences between the calculated and measured characteristics come from the deep saturation of the SRM, the incomplete material setting, error in measuring devices and the inaccurate measure of the dimensions [20].

An experimental setup has been implemented to drive the SRM in order to verify and study its performance. The benchmark layout is shown in Fig. 21. An experimental tests have been carried out as following:

1. A balanced motor operation.
2. Unbalanced motor operation; with phase A disconnected.
3. Unbalanced motor operation; with phase C reversed.

Figure 22 to Fig.24 illustrates the speed of the motor in each case. The current in each phase of the motor and the line supply current are shown in Fig.25 to Fig.27. Fig.28 to Fig.30 show the steady-state voltages that are applied on each phase of the motor through the IGBT converter, and also the supply voltage waveform. It is very clear that the supply is too weak according to its voltage variation. It is necessary to connect a capacitor in parallel with the supply to enforce its voltage and regenerate the power again. The induced voltages on the search coils (installed on the motor poles) are shown in Fig.31 to Fig.33, while the flux linkage waveforms are illustrated in Fig.34 to Fig.36. The shifted flux waveforms come from the RC gain of the integrator circuit. The flux waveforms are in triangles shape.

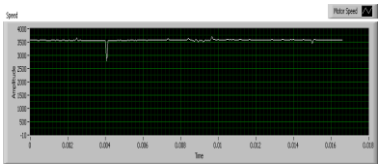

Fig. 22 motor speed in balanced operation.

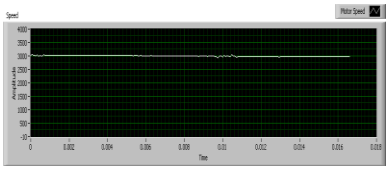

Fig. 23 motor speed in Unbalanced operation; with phase A disconnected.

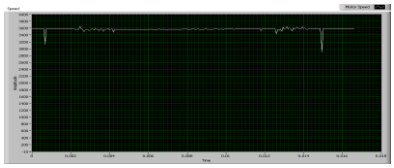

Fig. 24 motor speed in Unbalanced operation; with phase C reversed.

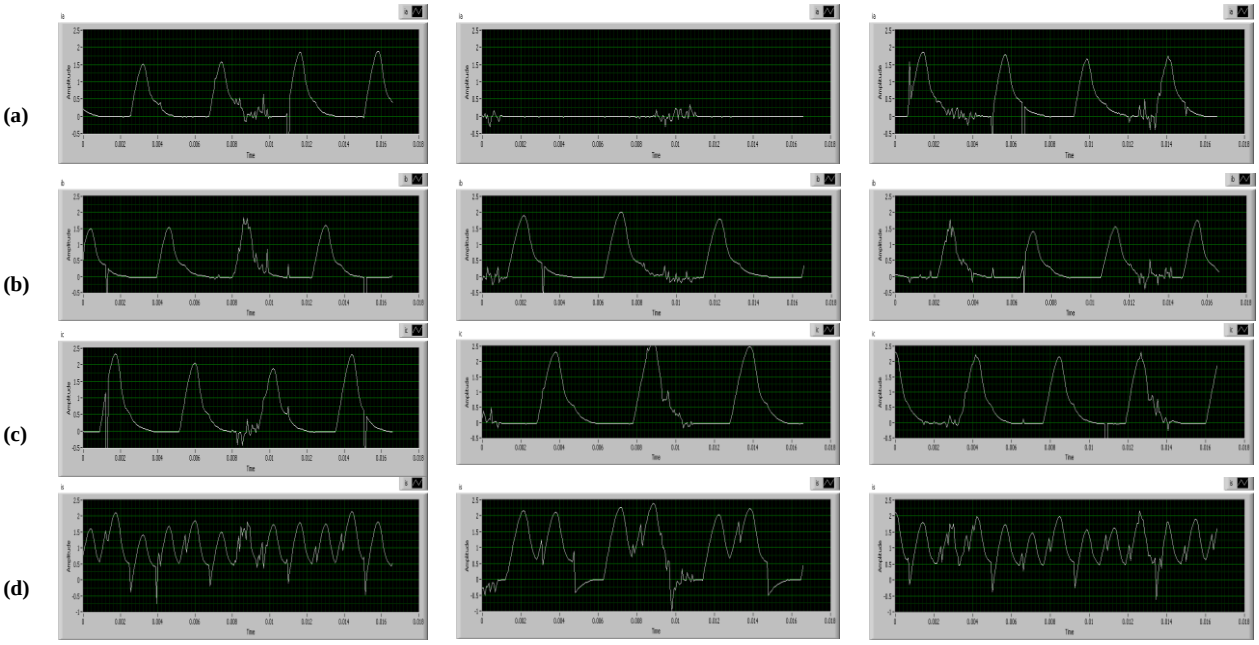

Fig. 25 motor current in balanced operation.
(a) Phase A current,
(b) Phase B current,
(c) Phase C current,
(d) Supply current.

Fig. 26 motor current in Unbalanced operation; with phase A disconnected.
(a) Phase A current,
(b) Phase B current,
(c) Phase C current,
(d) Supply current.

Fig. 27 motor current in Unbalanced operation; with phase C reversed.
(a) Phase A current,
(b) Phase B current,
(c) Phase C current,
(d) Supply current.

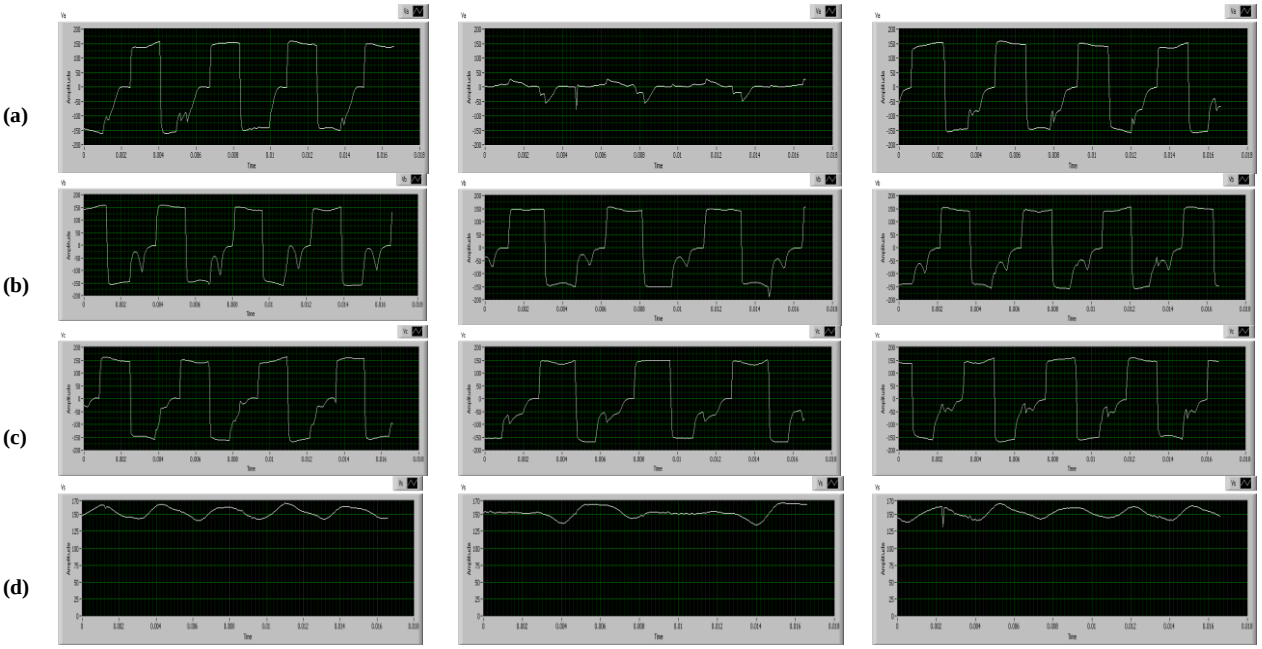

Fig.28 applied voltage in balanced operation.
(a) Phase A voltage,
(b) Phase B voltage,
(c) Phase C voltage,
(d) Supply voltage.

Fig. 29 applied voltage in Unbalanced operation; with phase A disconnected.
(a) Phase A voltage,
(b) Phase B voltage,
(c) Phase C voltage,
(d) Supply voltage.

Fig. 30 applied voltage in Unbalanced operation; with phase C reversed.
(a) Phase A voltage,
(b) Phase B voltage,
(c) Phase C voltage,
(d) Supply voltage.

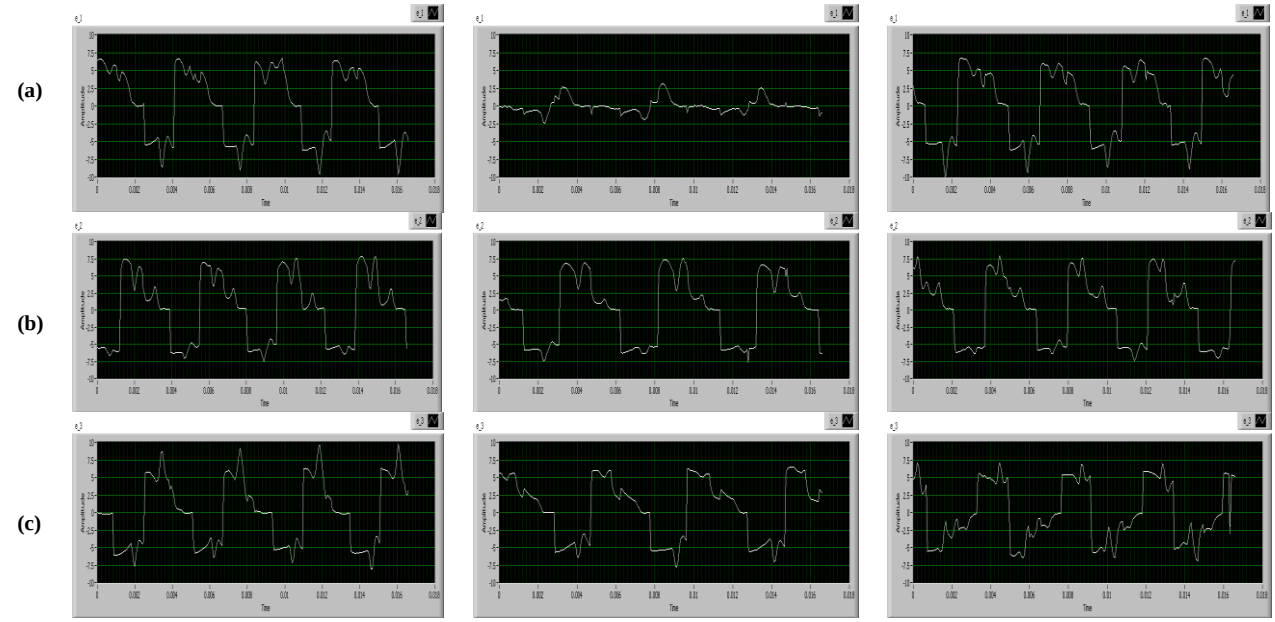

Fig. 31 induced voltage in balanced operation
(a) Phase A induced voltage,
(b) Phase B induced voltage,
(c) Phase C induced voltage,

Fig. 32 induced voltage in Unbalanced operation; with phase A disconnected.
(a) Phase A induced voltage,
(b) Phase B induced voltage,
(c) Phase C induced voltage,

Fig. 33 induced voltage in Unbalanced operation; with phase C reversed.
(a) Phase A induced voltage,
(b) Phase B induced voltage,
(c) Phase C induced voltage,

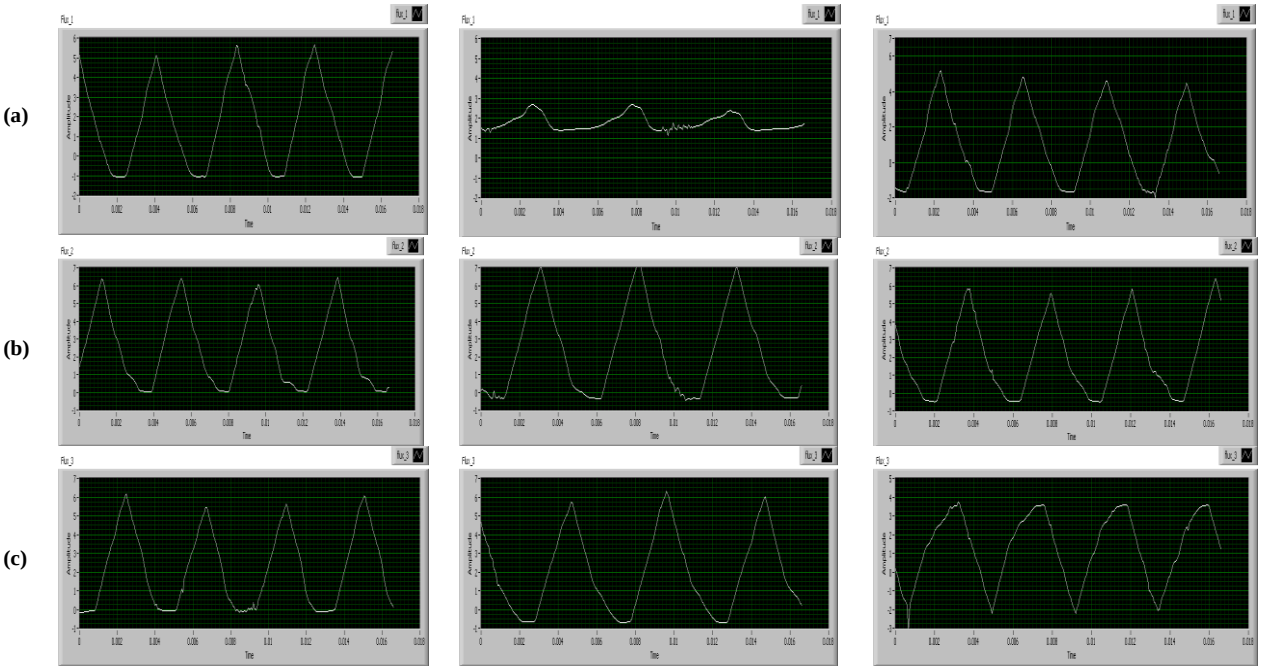

Fig. 34 flux waveforms in balanced operation.
(a) Phase A flux,
(b) Phase B flux,
(c) Phase C flux.

Fig. 35 flux waveforms in Unbalanced operation; with phase A disconnected.
(a) Phase A flux,
(b) Phase B flux,
(c) Phase C flux.

Fig. 36 flux waveforms in Unbalanced operation; with phase C reversed.
(a) Phase A flux,
(b) Phase B flux,
(c) Phase C flux.

The no-load speed of the motor in the balanced (normal) operation is 3600 rpm. The disconnection of one phase of the motor is a commonly occurrence condition. After the disconnection of phase A of the motor, the produced torque is reduced and the speed is decreased to be 3050 rpm. The motor current of the remaining healthy phases increases to regain the motor speed. The increased current affects the flux to increase also.

The torque does not depend on the current direction, but the direction of the current affects the magnetic circuit structure of the motor. In the third case, phase C of the motor is connected in reversed polarity to compose reversed magnetic poles. The speed in this case is nearly the same, but the current of the reversed phase is increased from the two phases. The flux of phase C is seen to be reversed shape triangles.

IX. Conclusions

The stator and rotor pole shapes have the main effect on the SRM performance from which, the torque ripple has been reduced. In this paper, the influence of both the stator and the rotor pole shoes for 6/4 SRM is investigated. The static characteristics are calculated by using 2D-FEM. The steady state characteristics are calculated by described machine's model using matlab/Simulink. The results illustrates that the addition of the stator pole shoe produces greater torque with ripple reduction, on the other hand, the addition of rotor pole shoe controls the inductance pattern and allows a significant reduction of the torque ripple. The proposed model saves the total laminated steel and copper materials compared with the increased pole width, this in turn reflects the low cost for industrial applications. The modified SRM is more efficient except for high speeds because it requires the controller to be adapted to the new inductance pattern by optimizing the turn-on

and off times. The estimated core losses for the proposed and standard SRMs are very close to be compared. Implementation of the SRM drive circuit is presented, and the dynamic results are illustrated and discussed.

References

[1] N. K. Sheth and K. R. Rajagopal, "Optimum pole arcs for a switched reluctance motor for higher torque with reduced ripple," IEEE Trans. on Magnetics, vol. 39, No. 5, pp. 3214–3216, September 2003.

[2] R. Krishnan Switched Reluctance Motor Drives. Boca Raton, FL: CRC Press, 2001.

[3] Z. Xu, D. Lee, J. Ahn," Analysis and Control of a Novel Bearingless Switched Reluctance Motor with Hybrid Stator Poles," Industrial Technology (ICIT), IEEE International Conference, pp.247–252, February 2013.

[4] T.J.E. Miller, "Optimal Design of Switched Reluctance Motors", IEEE Trans. on Industrial Electronics, vol. 49, No. 1, pp. 15–27, February 2002.

[5] I. Husain, "Minimization of torque ripple in SRM drives," IEEE Trans. on Industrial Electronics, vol. 49, No. 1, pp. 28–39, February 2002.

[6] V. Vujiˇcić, "Minimization of Torque Ripple and Copper Losses in Switched Reluctance Drive," IEEE Trans. on Power Electronics, vol. 27, No. 1, pp. 388–399, JANUARY 2012

[7] M. Balaji and V. Kamaraj, "Optimum design of switched reluctance machine using adaptive particleswarm optimization," ARPN Journal of Engineering and Applied Sciences , VOL. 7, No. 6, pp. 666-671, JUNE 2012.

[8] R.T.Naayagi , V.Kamaraj, "Modeling and design of shape optimized SRM with reduced ripple," IEEE International Conference on Emerging Technologies, pp.399-404, Islamabad, September 2005.

[9] T. Jahangiri, M. R. Feyzi and M. B. B. Sharifian ,"Finite element analysis of switched reluctance motor be control of firing angles for torque ripple minimization," Australian Journal of Basic and Applied Sciences, vol. 5, No. 9 , pp. 1391-1402, 2011.

[10] N. K. Sheth and K. R. Rajagopal, "Torque profiles of a switched reluctance motor having special pole face shapes and asymmetric stator poles IEEE Trans. on Magnetics, vol. 40, No. 4, pp.2035 – 2037, JULY 2004.

[11] Y. K. Choi, H. S. Yoon, C. S. Koh, "Pole-shape optimization of a switched-reluctance motor for torque ripple reduction," IEEE Trans. on Magnetics, vol. 43, No. 4, pp. 1797-1800, APRIL 2007

[12] J. W. Lee, H. S. Kim, B. I. Kwon, and B. T. Kim,"New rotor shape design for minimum torque ripple of SRM using FEM," IEEE Trans. on Magnetics, vol. 40, No. 2, pp. 754–757, Mar. 2004.

[13] F. Kentli, H. Çalik, "Matlab-simulink modelling of 6/4 srm with static data produced using finite element method," Acta Polytechnica Hungarica vol. 8, No. 6, 2011.

[14] D. UYGUN, C. AKÜNER and M. YUMURTACI, "A new construction of switched reluctance motor improving magnetic field energy and torque production". the 6th WSEAS International Conference on Applications of Electrical Engineering, Istanbul, Turkey, pp. 178 –182, May 2007.

[15] S. Sadeghi, M. Mirsalim, "Dynamic modeling and simulation of a switched reluctance motor in a series hybrid electric vehicle," Acta Polytechnica Hungarica vol. 7, No. 1, 2010.

[16] Vikas S. Wadnerkar, Dr. G. Tulasi Ram Das and Dr. A.D.Rajkumar," ERFORMANCE ANALYSIS OF SRM DRIVE USING

ANN BASED CONTROLLING OF 6/4 SWITCHED RELUCTANCE MOTOR", Journal of Theoretical and Applied Information Technology, pp. 334–338, 2009.

[17] M. Torrent, P. Andrada, B. Blanque, E. Martinez, J. I. Perat and J. A. Sanchez," Method for estimating core losses in switched reluctance motors" European Transactions on Electrical Power, vol. 21, No. 1, pp. 757–771, January 2011.

[18] J. Faiz, B. Ganji, C. E. Carstensen, and R. W. De Doncker,"Loss prediction in switched reluctance motors using finite element method", European Transactions on Electrical Power, vol. 19, No. 5, pp. 731–748, March 2008.

[19] P. Zhang, P.A. Cassani and S.S. Williamson, "An accurate inductance profile measurement technique for switched reluctance machines," IEEE Trans. on Industrial Electronics, VOL. 57, No. 9, pp. 2972 –2979, September 2010.

[20] K. Kiyota, T. Kakishima, H. Sugimoto, and A. Chiba ," Comparison of the test result and 3d-fem analysis at the knee point of a 60 kw srm for a HEV ," IEEE Trans. on Magnetics, vol. 49, No. 5, pp. 2291–2294, May. 2013.

Appendix

Table I: The Standard Machine Dimensions in [mm].

Geometry parameter	*symbol*	*Value*
Output power [Kw]	P_{out}	1.1
Rated speed [rpm]	n	800
Shaft radius	R_{sh}	19.05
Rotor outside radius	R_{oc}	30.5
Stator outside radius	R_{oy}	82.5
Stator yoke width	b_y	12.5
rotor yoke width	b_c	11.45
Air gap length	L_g	0.25
Height of stator pole	h_{ts}	25.28
Height of rotor pole	h_{tr}	13.7
Rotor pole arc angle [°]	β_r	33
stator pole arc angle [°]	β_s	30
Core length	L_a	103
Turns per phase	N	400
Phase resistance [Ω]	R	2.2
Core material	M19-steel	–
Lamination fill factor	–	1.0

TABLE II: Operating Conditions With Only Current Limiter.

Operating parameter	*SRM configuration*	
	Standard	*Proposed*
Supply Voltage [V]	240	240
Load torque [Nm]	11.5	11.5
Switch-on angle θ_{on} [°]	0	0
Switch-off angle θ_{off} [°]	Optimized to minimize torque ripple.	

TABLE III: Operating conditions with speed controller.

Operating parameter	*SRM configuration*	
	Standard	*proposed*
Supply Voltage [V]	240	240
Load torque [Nm]	10	10
Reference speed [rpm]	750	750
Switch-on angle θ_{on} [°]	0	0
Switch-off angle θ_{off} [°]	Optimized to minimize torque ripple.	